Characterization of ultra-shallow junctions using frequency-dependent junction photovoltage and its lateral attenuation

V.N. Faifer and M.I. Current

Frontier Semiconductor, San Jose, CA 95112

D.K. Schroder

Dept. of Electrical Engineering, Arizona State University, Tempe, AZ 85287-5706

Abstract

A contactless method for ultra-shallow junction (USJ) characterization is described based on analysis of frequency-dependent junction photovoltages from illuminated and non-illuminated areas. Relevant equations for junction photovoltages are derived. It is shown that the measured leakage current in USJ formed in halo profiles is related to space-charge region recombination

The requirement for source-drain extension (SDE) junction depths <10 nm to control short-channel effects for <30 nm gates [1], has accelerated the development of methods for activation annealing, based on laser scans or "flash" light pulses, and junction monitoring metrology.

One-dimensional frequency-domain characterization of semiconductors parameters was discussed in [2-5]. A rigorous two dimensional, non-steady-state junction photovoltage (JPV) method was developed in [5,6] and implemented for measuring sheet resistance (R_S) and leakage current (I_0) in p-n junctions. In [5,6] good correlation of this non-contact technique and standard four-point probe (4PP) was demonstrated for deep (junction depth > 50 nm) and low-leakage current p-n junctions. In the case of USJ formed in heavily doped regions, e.g., halo or pocket doping, practically no correlation between JPV and 4PP methods was observed due to probe penetration and high leakage currents in p-n junctions [6].

The present paper outlines an algorithm and theoretical background of a 2D frequency-dependent JPV method for USJ characterization and describes the mechanisms responsible for the leakage current. The basis of the measurement is to use photo-excitation of carriers in the p-n junction and wafer substrate and to monitor, in a spatially resolved manner, the JPV signals inside and outside the illumination area. Two electrodes, a round transparent electrode (1) with diameter $2r_0$ at the center of the probe and second round arc conducting electrode (2) subtending an angle β and coaxial with first electrode some small distance away, are used for measurements of JPV voltages V_1 and V_2, respectively (Fig. 1(a)(b)) [5].

Continuity and Poisson's equations were used to derive the 2-dimensional JPV distribution, $v(x,y,t)$, and to obtain the voltages V_1 and V_2. Operating in the low-light excitation regime, where

$v(x,y,t) << kT/q$, where k is Boltzmann's constant, T the Kelvin temperature, the junction photovoltage is proportional to the absorbed light flux and the variation of the surface space-charge region width, W, induced by illumination is smal1, allowing use of the one-dimensional Poisson equation at each point. By integration of the three-dimensional continuity equation over the vertical spatial coordinate, z, measured from the wafer surface ($0<z<x_j+W$) and using a solution of the 1D Poisson equation with assumption for substrate sheet resistance $R_{SSUB} << R_S$, we obtain the 2D equation for the photovoltage distribution

$$\frac{\partial^2 v}{\partial x^2} + \frac{\partial^2 v}{\partial y^2} = R_S \cdot C_{p-n} \cdot \frac{\partial v}{\partial t} + R_S \cdot G_{p-n} \cdot v \ - q \cdot \eta \cdot \Phi \cdot (1-R) \cdot R_S \qquad (1)$$

where Φ is the light flux, η the efficiency, R the reflectivity, and R_s, C_{p-n}, G_{p-n} the pn junction sheet resistance, capacitance and conductance.

In the case of harmonic modulation of the light intensity, $\Phi(t) = \Phi_0(x,y)(1-\cos(2\pi ft))$, the junction photovoltage is $v(x,y,t) = v_0(x,y)*\cos(2\pi ft+\varphi(x,y))$. By solving Eq. (1) and taking integral inside the illumination area, $r<r_0$ we determine the photovoltage signal from the circular transparent and conducting electrode as

$$V_1 = \frac{q\eta(1-R)\Phi_0 R_S}{k^2}\left[1 - \frac{2}{kr_0}\frac{I_1(kr_0)K_1(kr_0)}{I_0(kr_0)K_1(kr_0) + I_1(kr_0)K_0(kr_0)}\right] \qquad (2)$$

By taking the integrals outside the illumination area, $r_0<r_1<r<r_2$ we get the photovoltage from partially round arc conducting electrode subtending an angle β (Fig.1b)

$$V_2 = q\eta \frac{(1-R)\Phi_0 \beta R_S}{\pi \cdot k^3 r_0^2} \frac{I_1(kr_0)\left[r_1 K_1(kr_1) - r_2 K_1(kr_2)\right]}{I_0(kr_0)K_1(kr_0) + I_1(kr_0)K_0(kr_0)} \tag{3}$$

where $I_0(z)$, $I_1(z)$ and $K_0(z)$, $K_1(z)$ are the modified Bessel functions and

$$k = \sqrt{R_S G_{p-n} + i2\pi f R_S C_{p-n}} \ . \tag{4}$$

The junction conductance, $G_{p\text{-}n}$, and leakage current density, I_0, are related by $G_{p\text{-}n} = I_0 q/kT$. The theoretical frequency-dependent JPV voltage V_1 for 1D [4] and 2D algorithms and JPV voltage V_2 for the 2D algorithm are shown in Fig.2. For very high sheet resistance, $R_s >> 10^6$ ohms/square, the 2D curves coincide with the 1D curve [4] (Fig.2a). With decreasing sheet resistance, the 2D photovoltage decreases and the curves no longer have distinct corner frequencies like the 1D curve [4].

By measuring the JPV at the two electrodes at different frequencies, combined with reference JPV measurements on a wafer with a deep p-n junction with known sheet resistance, the sheet resistance, R_s, conductance $G_{p\text{-}n}$ and capacitance of the p-n junction, $C_{p\text{-}n}$ can be simultaneously determined using measured voltages V_1 and V_2 and Eqs. (2) and (3).

The sheet resistance and leakage current of a laser annealed boron doped $p^{++}n$ USJ formed in an As-doped ($N_D \approx 10^{19}$ cm^{-3}) halo profile was measured. The experimental (points) and theoretical (curves) JPV voltages V_1 and V_2 versus frequency are shown in Fig. 3. The measured sheet resistance and leakage current in USJ #1 are R_s=423 ohms/square and $I_0 = 10^{-6}$ A/cm^2. USJ

#2 is very leaky with I_0=2.5x10^{-2}A/cm^2 and as a result, JPV signal V_2 being less than the noise voltage $V_2 < V_{noise} \approx 0.3$ mV, the JPV voltage V_2 is not shown in Fig. 3 and the sheet resistance of the second wafer was not determined.

This example demonstrates that rapid laser annealing can lead to high leakage current. Under illumination, the p-n junction is forward biased and the band-to-band tunneling effect is small since halo is not degenerate (i.e., Fermi level in halo is still within band gap). The measured leakage current is determined by diffusion and recombination of excess carriers in the bulk, J_{diff}, recombination at the surface, J_S, and in the space-charge region with trap assisted tunneling (TAT), J_W . In the case of uniform traps, an approximate expression is [4, 7, 8]

$$J_{leak} = J_{diff} + J_S + J_W \approx q\frac{n_i^2}{N_D}\sqrt{\frac{D_p}{\tau_p}} + qs_r\frac{n_i^2}{N_A} + \frac{qn_iW(1+\Gamma)}{\tau_g} \tag{5}$$

where N_A, N_D are the acceptor and donor densities in the top layer of p-n junctions and in the halo profiles near the p-n junction, τ_g the generation lifetime in the pn junction space-charge region, D_p and τ_p holes diffusivity and lifetime in n-type halo profiles, W the space-charge region width, n_i the intrinsic carrier density, s_r the surface recombination velocity, Γ is TAT factor.

For doping densities $N_A \approx 10^{21}$ cm^{-3}, $N_D \approx 5\text{x}10^{18}$ cm^{-3} and maximum surface recombination velocity and diffusion velocity equal to the thermal velocity $s_r = (D_p/\tau_p)^{0.5} = v_{th} \approx 10^7$ cm/s, the bulk and surface recombination contribution $J_{diff} + J_s \approx 10^{-10}$ A/cm^2 is very low compared to the measured leakage current and the space-charge region recombination current, J_W, dominates.

We compare the reverse-bias leakage current measured by the standard contact technique with this non-contact JPV technique. The leakage current in heavily-doped p-n junction under reverse bias includes two additional components: band-to-band tunneling current, J_{tun}, [9] and thermionic emission current, J_{them} [10]. In the case of heavily-doped halo (~5x10^{18} cm^{-3}) and abrupt USJ, the band-to-band tunnel current density is $J_{tun} \approx 10^{-4}$ A/cm^2 [9], which sets the lower leakage current limit for the case of moderate trap densities. For this reason, the reverse-biased leakage current is sensitive to trap density in space charge region until $J_{tun} > J_W$. When the trap concentration is high and $J_{tun} < J_W$, the reverse-biased leakage current is proportional to the concentration of re-combination centers in the space-charge region. We believe that the main contribution to J_W is related to insufficiently annealed end-of-range damage located in space-charge region which can result in high carrier trap concentrations. Leakage current measurements for heavily doped (>10^{18} dopants/cm^3) substrates and halo profiles are consistent with carrier trap densities ranging from N_{trap}~10^{15} to >10^{18} traps/cm^3 and traps capture cross section $\sigma=10^{-14}$ cm^2 [6].

In conclusion, we demonstrate a contactless 2 dimensional frequency-dependent JPV method for USJ characterization. The key benefit of this method is the ability to obtain separate measurements of sheet resistance and leakage current, independent of junction depth without the need for pre-measurement surface preparation. The measured leakage current is directly linked to space-charge region recombination.

ACKNOWLEDGMENTS

The authors acknowledge Ann Koo for support of this project T.M.H. Wong and G. Mikhailov for discussions.

References

1. See Table 69 in the Front End Process section of the ITRS05. www.itrs.net.
2. D.K. Schroder, J.E. Park, B.D. Choi, S. Kishino, and H. Yoshida, *IEEE Trans. Electron Dev*., **47,** 1653-1661 (2000).
3. R.S. Nakhamson, *Solid State Electron*., **18**, 617-626 (1975).
4. J.E. Park, D.K. Schroder, S.E. Tan, B.D. Choi, M. Fletcher, A. Buczkowski, F. Kirscht, *J. Electrochem. Soc*., **148**, G411-G419 (2001).
5. V.N. Faifer, M.I. Current, W.J. Walecki, V.V. Sushkov, G. Mikhailov, P. Van, T. Nguyen, T.M.H. Wong, J. Lu, S.H. Lau and A. Koo., *Mat.Res.Soc. Symp. Proc*. **810**, 475-480. (2004).
6. V.N. Faifer, M.I. Current, T.M.H. Wong, and V.V. Souchkov, *J. Vac. Sci. Technol*. **B24**, 414-420 (2006).
7. G.A.M. Hurkx, D.B.M. Klassen, and M.P. Knuvers, *IEEE Trans. Electron Dev*. **39**, 2090-2098 (1992).
8. J.E. Park, J. Shields, and D.K. Schroder, *Solid-State Electron*., **47**, 855-864 (2003).
9. P. M. Solomon, D.J. Frank, J. Jopling, C. D'Emic, O. Dokumaci, P. Ronsheim, and W.E. Haensch, IEEE IEDM, 9.3.1-9.3.4 (2003).
10. R. Lindsay, K. Henson, W. Vandervorst, K. Maex, B. J. Pawlak, R. Duffy, R. Surdeanu, P. Stolk, J. A. Kittl, S. Giangrandi, X. Pages, and K. van der Jeugd , *J. Vac. Sci. Technol.* **B22**, 306-311 (2004).

Figure captions.

Figure 1. (a) Photo-excitation and carrier drift with a modulated light source and two capacitor electrodes for monitoring the induced junction photovoltage in a spatially resolved manner; (b) electrode configuration.

Figure 2. JPV voltages V_1 (a) and V_2 (b) versus frequency calculated for 1D (infinite sheet resistance) and for 2D as function of sheet resistance ($Cp\text{-}n$=5x10^{-9} F/cm^2, I_0=2.6x10^{-6} A/cm^2).

Figure 3. JPV voltages V_1 *and* V_2 (points) and theoretical values (curves) versus light modulating frequency for USJ #1 (good p-n junction) and USJ #2 (leaky p-n junction).

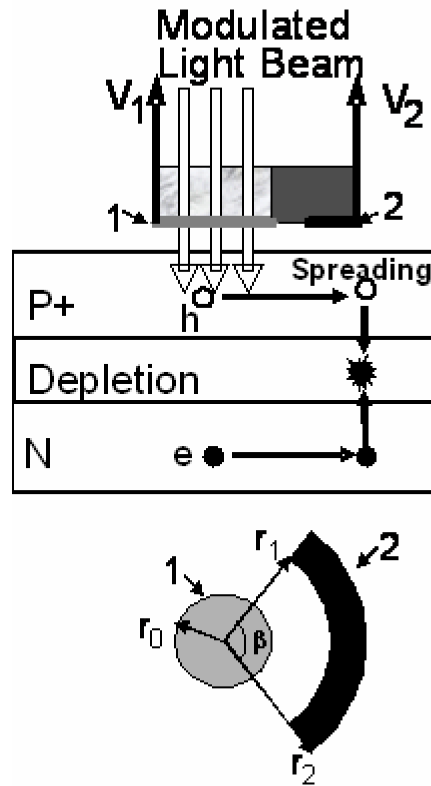

Figure 1. (a) Photo-excitation and carrier drift with a modulated light source and two capacitor electrodes for monitoring the induced junction photovoltage in a spatially resolved manner; (b) electrode configuration.

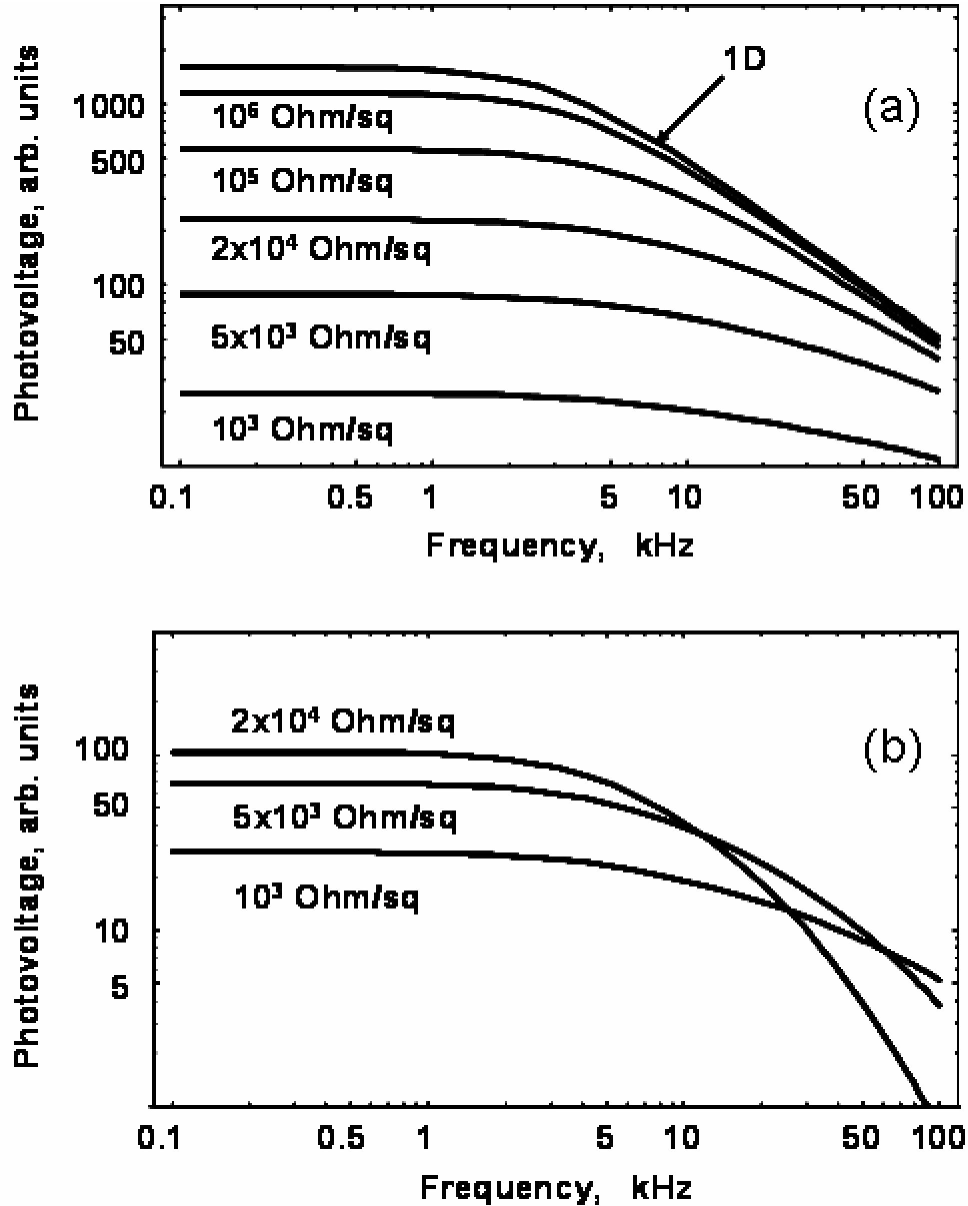

Figure 2. JPV voltages V_1 (a) and V_2 (b) versus frequency calculated for 1D (infinite sheet resistance) and for 2D as function of sheet resistance ($C_{p\text{-}n}$=5x10^{-9} F/cm^2, I_0=2.6x10^{-6} A/cm^2).

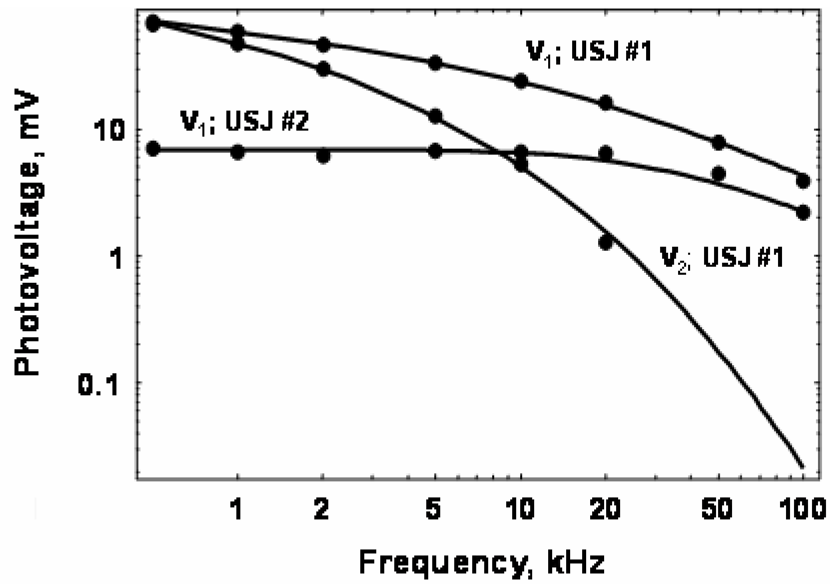

Figure 3. JPV voltages *V_1 and V_2* (points) and theoretical values (curves) versus light modulating frequency for USJ #1 (good p-n junction) and USJ #2 (leaky p-n junction).